International Journal of Thermophysics, Vol. 18, No. 6, 1997

An Equation of State for the Thermodynamic Properties of R143a (1,1,1-Trifluoroethane)

S. L. Outcalt[1,2] and M. O. McLinden[1]

Received April 1, 1997

Thermodynamic properties of 1,1,1-trifluoroethane (R143a) are expressed in terms of a 32-term modified Benedict–Webb–Rubin (MBWR) equation of state. Coefficients are reported for the MBWR equation and for ancillary equations used to fit the ideal-gas heat capacity, and the coexisting densities and pressure along the saturation boundary. The MBWR coefficients were determined from a multiproperty fit that used the following types of experimental data: *PVT*; isochoric, isobaric, and saturated-liquid heat capacities; second virial coefficients; speed of sound and properties at coexistence. The equation of state was optimized to the experimental data from 162 to 346 K and pressures to 35 MPa with the exception of the critical region. Upon extrapolation to 500 K and 60 MPa, the equation gives thermodynamically reasonable results. Comparisons between calculated and experimental values are presented.

KEY WORDS: 1,1,1-trifluoroethane (R143a); equation of state; refrigerants; thermodynamic properties.

1. INTRODUCTION

This paper describes a 32-term modified Benedict–Webb–Rubin (MBWR) equation of state used to represent the thermodynamic properties of R143a. 1,1,1-Trifluoroethane (R143a) is a hydrofluorocarbon (HFC), which has zero ozone depletion potential since it does not contain chlorine. Because it is "ozone friendly," R143a (primarily in combination with pentafluoroethane (R125) and/or 1,1,1,2-tetrafluoroethane (R134a)) is being considered as a replacement for R22. (In accordance with the Montreal Protocol, R22 is mandated to be phased out of all but a few commercial applications by 2020.)

[1] Physical and Chemical Properties Division, National Institute of Standards and Technology, Boulder, Colorado 80303-3328, U.S.A.

[2] To whom correspondence should be addressed.

0195-928X/97/1100-1445$12.50/0

Experimental data of the following types were used to formulate the equation: single-phase pressure–volume–temperature (PVT), heat capacity, speed of sound, second virial coefficients, vapor pressure, saturated-liquid density, and saturated-vapor density. The equation was optimized to R143a properties data over a pressure range from 0 to 35 MPa and a temperature range from 162 to 346 K.

2. EXPERIMENTAL DATA

Tables I–III list the data that were available at the time of this fit. (All temperatures in this work are on the ITS-90; data that were measured on the IPTS-68 were converted to ITS-90 before the MBWR equation was fitted to the data.) The critical constants used in this correlation were $T_c = 346.04$ K [6], $\rho_c = 5.151118$ mol · L^{-1} (432.9 kg · m^{-3}) [6], and $P_c =$ 3.7756 MPa. The value used for the critical pressure was obtained by extrapolating the vapor pressure data of Weber and Defibaugh [13] to the critical temperature of Schmidt [6].

3. ANCILLARY EQUATIONS

Ancillary equations (and their derivatives) for vapor pressure, and saturated liquid and saturated vapor density are used by the MBWR fitting routine to calculate values for other thermodynamic properties. These

Table I. Reported Critical-Point Parameters and Triple-Point Temperature for R143a

Investigator(s)	Ref. No.	Temperature (K)	Pressure (MPa)	Density (mol · L^{-1})
Critical point				
Arnaud et al.	1	346.0 ± 0.1	3.787 ± 0.15	5.414 ± 0.059
Fukushima	2	345.97	3.769 ± 0.005	5.105 ± 0.036
Higashi and Ikeda	3	345.88 ± 0.01	3.763 ± 0.003	5.128 ± 0.036
Mears et al.	4	346.25 ± 0.5[a]	3.76 ± 0.07	5.16 ± 0.12
Nagel and Bier	5	345.75 ± 0.06	3.765 ± 0.006	5.081 ± 0.107
Schmidt	6	346.04 ± 0.02		5.151
Wang et al.	7	346.18 ± 0.05	3.780 ± 0.006	5.259 ± 0.048
Triple point				
Magee	8	161.34 ± 0.02		
Russell et al.	9	161.82 ± 0.04[a]		

[a] The temperature in the source paper was on an unspecified scale and is reported here without any conversion.

Table II. Summary of Saturation and Ideal-Gas Heat Capacity Data for R143a

Investigator(s)	Ref. No.	No. of points used total	Temperature range (K)	Dev. from anc. eq. (%) Bias	A.A.D.
Vapor pressure					
de Vries	10	55 59	222 345	0.024	0.026
Giuliani et al.	11	0 61	244 – 346	[−0.036][a]	[0.080]
Giuliani et al.	12	0 16	304 345	[0.122]	[0.122]
Magee	8	13 13	165–225	−0.026	0.045
Mears et al.	4	0 7	226 344	[0.319]	[0.397]
Nagel and Bier	5	0 26	205 346	[0.324]	[0.324]
Russell et al.	9	0 9	173–226	[0.586]	[0.586]
Wang et al.	7	0 30	313 346	[−0.096]	[0.096]
Weber and Defibaugh	13	52 52	236–343	−0.020	0.026
Saturated liquid density					
Defibaugh and Moldover	14	0 20	243–343	[0.087]	[0.139]
Magee[b]	8	9 10	164 335	0.008	0.024
Mears et al.	4	0 6	298–338	[3.485]	[3.485]
Yokoyama and Takahashi	15	2 16	248–341	−0.031	0.207
Saturated vapor density					
Gillis[c]	16	13 16	170–320	−0.009	0.029
Holcomb	17	2 5	281 340	−0.552	1.758
Ideal-gas heat capacity					
Chen et al.	18	3 18	150 1500	0.025	0.065
Gillis	15	8 8	250 400	−0.009	0.150
Mears et al.	4	0 9	200–1000	[−3.973]	[4.323]
Smith and Brown	19	0 4	250–600	[0.035]	[0.644]
Vanderkooi and De Vries	20	0 1	300	[−10.012]	[−10.012]

[a] Data in brackets not used in fit.
[b] Calculated from isochoric P/T data of Magee.
[c] Calculated from virial coefficients of Gillis.
[d] Calculated from C_σ data of Magee.

ancillary equations are used only as an aid in fitting and are independent of the final MBWR equation. The ancillary equation for vapor pressure is

$$\ln\left[\frac{P_\sigma}{P_c}\right] = \frac{\alpha_0\tau + \alpha_1\tau^{1.5} + \alpha_2\tau^2 + \alpha_3\tau^4 + \alpha_4\tau^{6.5}}{1-\tau} \tag{1}$$

and those for saturated-liquid and saturated-vapor densities are

$$\rho_L = \rho_c(1 + d_0\tau^\beta + d_1\tau^{2/3} + d_2\tau + d_3\tau^{4/3}) \tag{2}$$

$$\rho_V = \frac{P_\sigma}{RT}\left[\left[\left[1 + \frac{f_0\tau^\beta + f_1\tau^{2\beta} + f_2\tau + f_3\tau^2 + f_4\tau^4}{1 + f_5\tau}\right]\frac{P_\sigma(Z_c - 1)}{P_c T_r^8}\right] + 1\right]^{-1} \tag{3}$$

Table III. Summary of *PVT*, Specific Heat, and Sound-Speed Data for R143a[a]

Source	No. of points used/total	Range of data			Dev. from MBWR (%)	
		T(K)	P(MPa)	ρ(mol·L^{-1})	Bias	A.A.D.
PVT						
Arnaud et al. [1]	0/40	293/363	0.6/3.0	0.29/1.36	n.a.[a]	n.a.
Defibaugh [14]	0/855	242/372	1.5/6.5	2.08/13.5	[0.338][b]	[0.338]
de Vries [10]	408/552	243/393	1.6/18.1	1.2/13.9	−0.036	0.048
Giuliani et al. [11]	0/14	273/363	0.5/0.8	0.29	[−0.081]	[−0.088]
Giuliani et al. [12]	0/62	268/363	0.5/4.1	0.26/5.1	[−0.480]	[0.685]
Magee [8]	144/144	166/400	3/35	8.5/15.8	0.034	0.039
Mears [4]	0/21	320/369	1.2/4.3	0.58/2.66	[−1.979]	[2.044]
Weber [13]	108/117	276/373	0.2/6.6	0.1/6.1	0.037	0.071
Isobaric heat capacity						
Russell et al. [9]	0/11	165/221	Sat. liq.		[0.009]	[0.197]
Isochoric heat capacity						
Magee [8], C_v	136/136	172/342	3.0/34.3	9.7/15.6	0.167	0.455
Magee [8], C_σ	83/84	165/343	Sat'n.	7.2/15.7	−0.145	0.145
Speed of sound						
Gillis [16]	171/178	235/400	0.04/1.1		0.00	0.02
Second virial coefficient						
Bignell and Dunlop [21]	0/3	290/310			[−0.649]	[0.649]
Gillis [16]	7/7	250/400			0.51	0.51

[a] n.a., not applicable. Data presented only graphically.
[b] Data in brackets not used in fit.

where T_c is the critical temperature, P_c is the critical pressure, ρ_c is the critical density, $\tau = 1 - (T/T_c)$, $R = 8.314471$ J·mol^{-1}·K^{-1} [22], $Z_c = P_c/(\rho_c R T_c)$, and $\beta = 0.325$. The equation for the saturated-vapor density is a form suggested by Friend et al. [23]. It approaches the ideal-gas limit at low temperatures and pressures and has the correct shape near the critical temperature. The coefficient f_0 is fixed by the d_0 term in the saturated-liquid density equation by $f_0 = d_0/(1 - (1/Z_c))$ ensuring that the saturated-liquid and saturated-vapor density curves join smoothly at the critical point. The MBWR fitting routine also requires an ancillary equation for ideal-gas heat capacity; we used

$$\frac{C_p}{R} = c_0 + c_1 T + c_2 T^2 + c_3 T^3 \tag{4}$$

Coefficients for the ancillary equations are listed in Table IV.

Table IV. Coefficients for Ancillary Eqs. (1)-(4)[a]

	0	1	2	3	4	5
a_i	−7.373 967	+2.052 859	−1.480 224	−3.033 281	+0.114 180	
d_i	+1.400 099	+2.655 041	−3.167 099	+2.021 717		
f_i	−0.478 680	−1.862 297	+0.0	+0.997 344	−0.365 505	+0.745 440
c_i	+1.838 736	$+3.019\,94 \times 10^{-2}$	$-1.784\,55 \times 10^{-5}$	$+4.424\,42 \times 10^{-9}$		

[a] Coefficients for Eq. (1) (3) are dimensionless; coefficients for Eq. (4) are for temperature in K.

The ancillary fit of the vapor pressure included data of de Vries [10], Weber and Defibaugh [13], and data generated from the saturated heat capacities C_σ of Magee [8]. (The method used to calculate vapor pressures from saturated-heat capacity data is a simple inverse of the method used by Weber [24] to estimate saturated heat capacities from vapor pressure data.) A plot of the deviations of experimental vapor pressures from those calculated by the ancillary equation is shown in Fig. 1. The data of Weber and Defibaugh [13] and of de Vries [10] agree within ±0.05% except below 240 K. The data of de Vries [10] are consistently higher than those of Weber and Defibaugh [13], but the magnitude of the differences

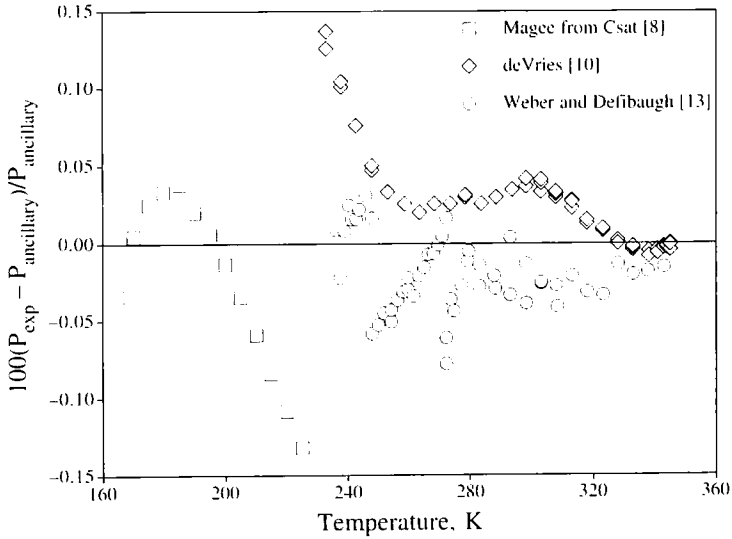

Fig. 1. Deviations of experimental vapor pressures from vapor pressures calculated with the ancillary equation [Eq. (1)].

decreases with increasing temperature. Deviations increase with increasing temperature for the data of Magee [8], because the assumptions made in the method used to calculate these vapor pressures are more nearly correct at low reduced temperatures and pressures (that is, at nearly ideal-gas conditions). Statistics for each of the data sets used in the fits of the ancillary equations are given in Table II.

The ancillary equation for saturated-liquid density was fitted with the data of Yokoyama and Takahashi [15] and densities extrapolated from the isochoric *PVT* data of Magee [8]. Figure 2 shows the deviations of the data used in the fit of the ancillary equation. The filled symbols represent the data of Magee [8] and Yokoyama and Takahashi [15] used in the fit, while the open symbols represent the data of the respective authors that were not used in the fit. Nine of the ten extrapolated saturated-liquid densities of Magee [8] are fitted very well (deviations no greater than $\pm 0.1\%$) by the ancillary equation. The tenth point (the highest temperature point) was not used in the formulation of the ancillary equation and has a deviation of 0.932% from that equation. The two highest temperature data points of Yokoyama and Takahashi [15] were included to prevent the equation from exhibiting erratic behavior near the critical point.

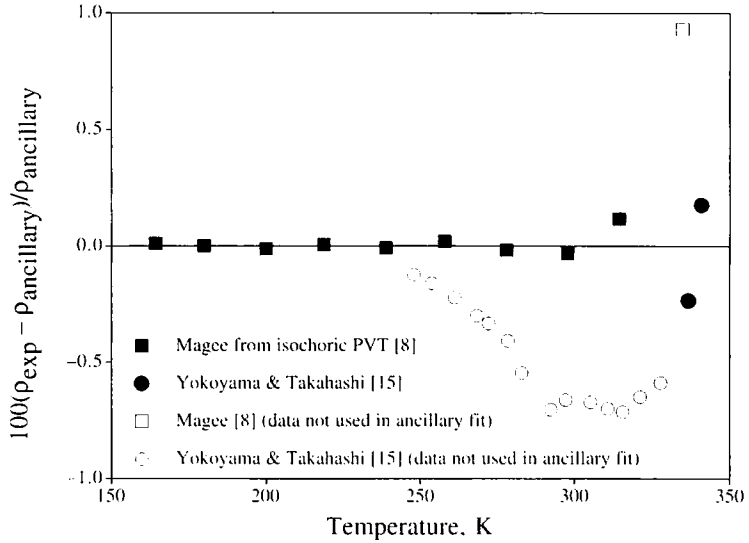

Fig. 2. Deviations of experimental saturated-liquid densities from saturated-liquid densities calculated with the ancillary equation [Eq. (2)].

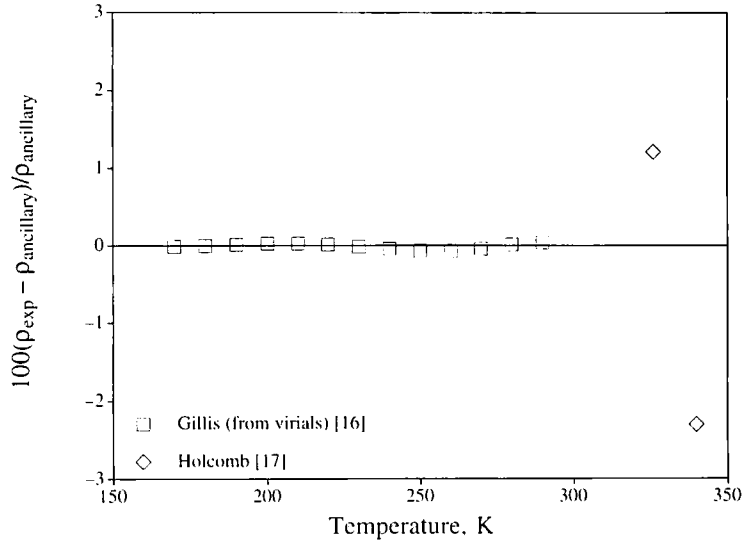

Fig. 3. Deviations of experimental saturated-vapor densities from saturated-vapor densities calculated with the ancillary equation [Eq. (3)].

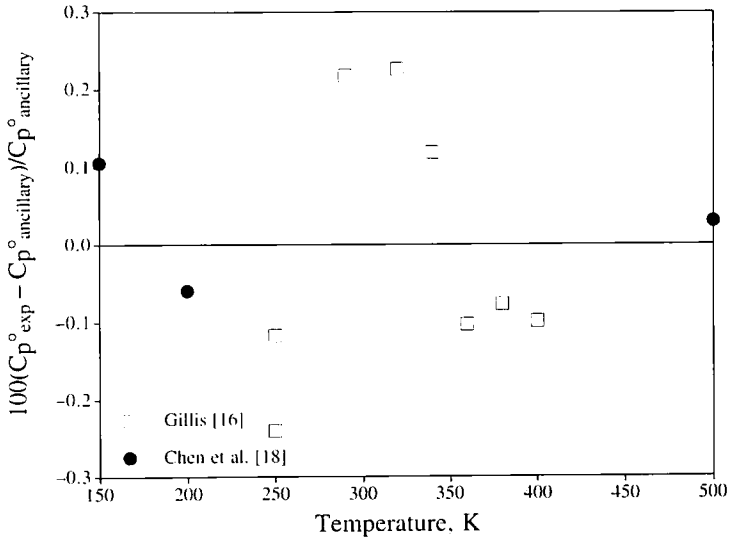

Fig. 4. Deviations of experimental ideal-gas heat capacities from ideal-gas heat capacities calculated with Eq. (4).

decreases with increasing temperature. Deviations increase with increasing temperature for the data of Magee [8], because the assumptions made in the method used to calculate these vapor pressures are more nearly correct at low reduced temperatures and pressures (that is, at nearly ideal-gas conditions). Statistics for each of the data sets used in the fits of the ancillary equations are given in Table II.

The ancillary equation for saturated-liquid density was fitted with the data of Yokoyama and Takahashi [15] and densities extrapolated from the isochoric *PVT* data of Magee [8]. Figure 2 shows the deviations of the data used in the fit of the ancillary equation. The filled symbols represent the data of Magee [8] and Yokoyama and Takahashi [15] used in the fit, while the open symbols represent the data of the respective authors that were not used in the fit. Nine of the ten extrapolated saturated-liquid densities of Magee [8] are fitted very well (deviations no greater than $\pm 0.1\%$) by the ancillary equation. The tenth point (the highest temperature point) was not used in the formulation of the ancillary equation and has a deviation of 0.932% from that equation. The two highest temperature data points of Yokoyama and Takahashi [15] were included to prevent the equation from exhibiting erratic behavior near the critical point.

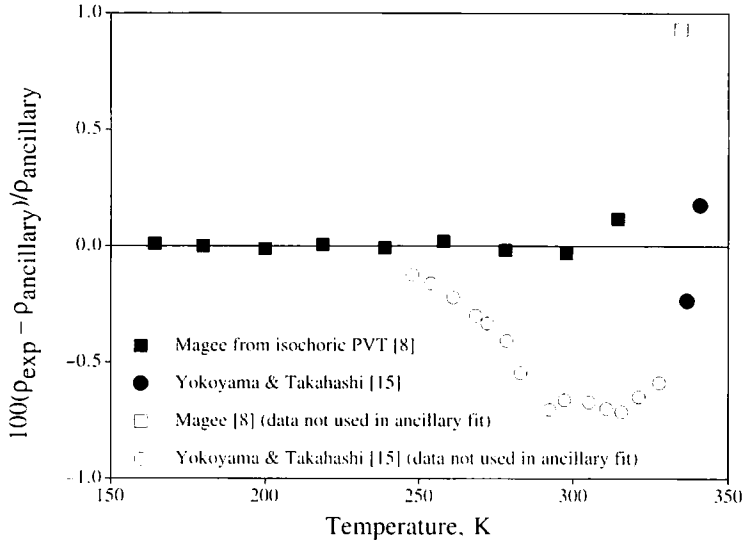

Fig. 2. Deviations of experimental saturated-liquid densities from saturated-liquid densities calculated with the ancillary equation [Eq. (2)].

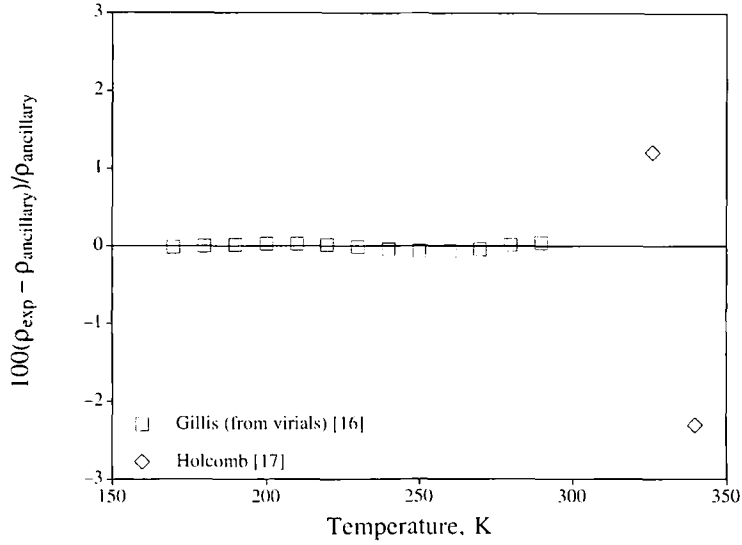

Fig. 3. Deviations of experimental saturated-vapor densities from saturated-vapor densities calculated with the ancillary equation [Eq. (3)].

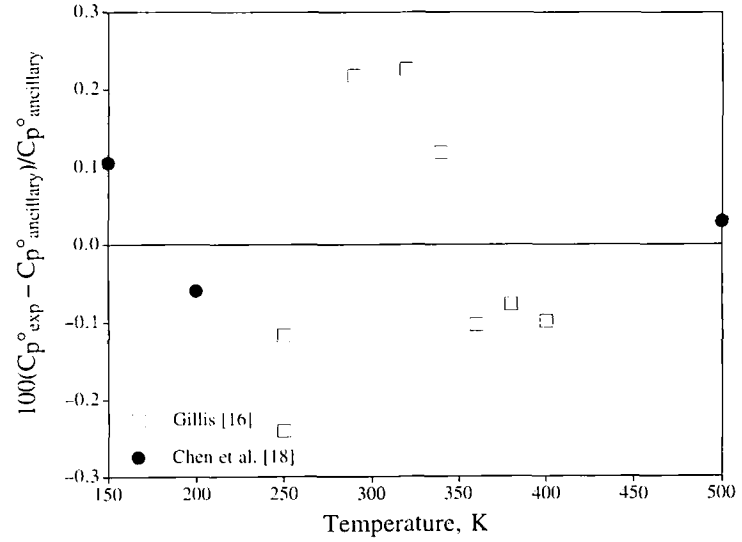

Fig. 4. Deviations of experimental ideal-gas heat capacities from ideal-gas heat capacities calculated with Eq. (4).

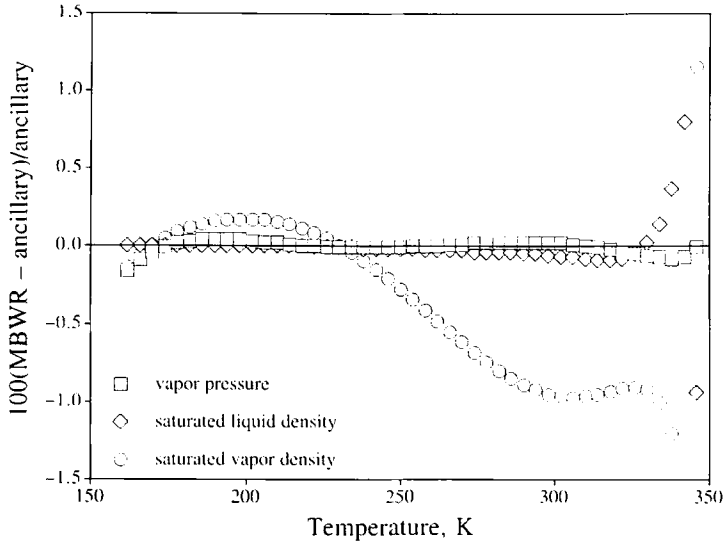

Fig. 5. Deviations of ancillary equations for vapor pressure, saturated-liquid, and saturated-vapor densities from values calculated with the MBWR equation.

saturated-liquid density is 0.071%, and that for saturated-vapor density is 0.308%. A.A.D. is defined by

$$\text{A.A.D.} = \frac{1}{n} \sum_{i=1}^{n} |100(x_{i,\text{exp}} - x_{i,\text{calc}})/x_{i,\text{calc}}| \tag{6}$$

5.2. Single-Phase PVT

Figures 6 and 7 show density deviations of experimental *PVT* data from the MBWR correlation. The overall fit of the *PVT* data used in the correlation of the MBWR equation has an A.A.D. of 0.39% and a bias of 0.34% for density, where bias is defined as

$$\text{bias} = \frac{1}{n} \sum_{i=1}^{n} |100(x_{i,\text{exp}} - x_{i,\text{calc}})/x_{i,\text{calc}}| \tag{7}$$

The 408 points of de Vries [10] that were used in the formulation cover both the liquid and the vapor regions and show small, but consistently negative density deviations (with respect to the MBWR equation) up to approximately 333 K. Above the critical temperature of R143a (346.04 K) the deviations of the de Vries [10] data become more scattered about 0.

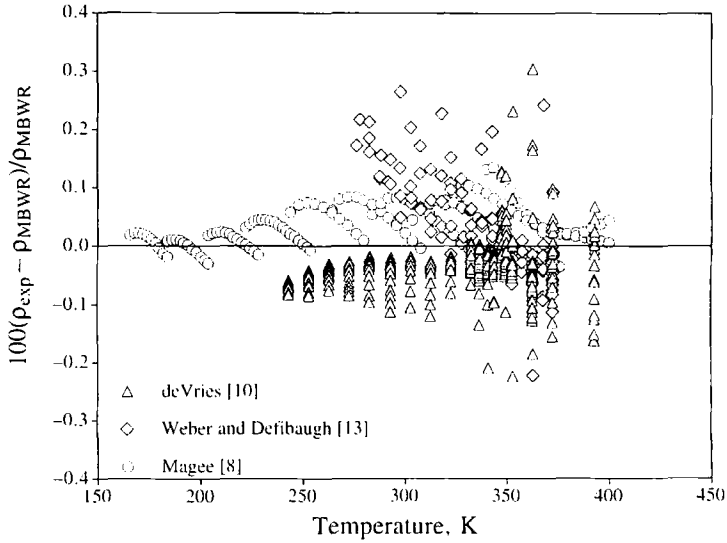

Fig. 6. Deviations of experimental *PVT* data used in the formulation of the MBWR equation from densities calculated with the MBWR equation as a function of temperature.

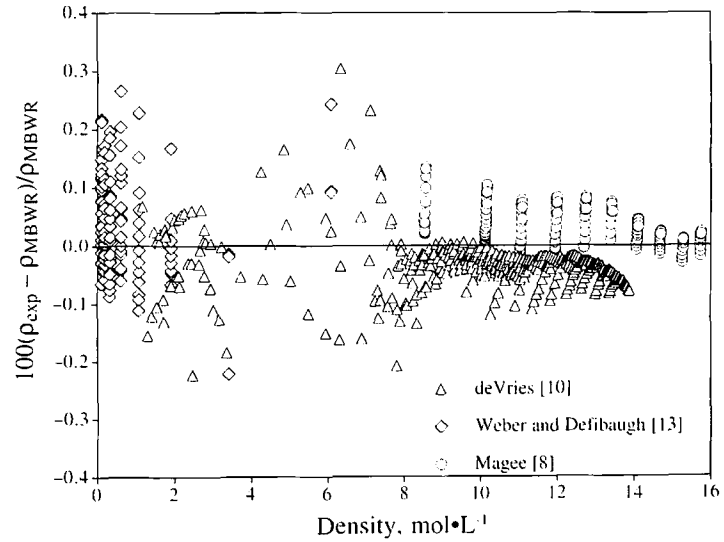

Fig. 7. Deviations of experimental *PVT* data used in the formulation of the MBWR equation from densities calculated with the MBWR equation as a function of experimental density.

The isochoric data of Magee [8] are all in the liquid phase, and all 144 points are fitted to within $\pm 0.15\%$. Density deviations of the Magee data are primarily positive. The biases of the Magee [8] data set and the de Vries [10] data set are approximately equal and opposite (see Table III). Thus the MBWR equation of state essentially splits the small difference between the two main *PVT* data sets used in the fit. Weber and Defibaugh's [13] data are also isochoric, but all in the vapor phase. The Weber and Defibaugh [13] data show greater deviations and more scatter about zero than the de Vries [10] or Magee [8] data. Because we do not intend to characterize the near-critical region with extreme accuracy, and because the MBWR equation of state, like any classical equation of state, is not well suited to fit that region, near-critical data are often excluded (or given very low weight) in order to avoid decreasing the accuracy of the fit in other regions. Seven of the nine Weber and Defibaugh [13] points not used in the correlation of the MBWR equation were along the highest density isochore ($6.07\ \text{mol} \cdot \text{L}^{-1}$). The data of de Vries [10] along the isotherms at 345, 346, and 347 K were not included in the MBWR equation formulation for this reason. Table III lists the A.A.D. and bias (in terms of density) for the *PVT* data sets.

Figures 8 and 9 show density deviations (of the available *PVT* data not used in the formulation of the MBWR equation for R143a) from the MBWR equation as a function of temperature and experimental density, respectively. These figures show that our MBWR equation for R143a represents the available experimental *PVT* data within approximately $\pm 1.5\%$ except for the 1955 data of Mears [4], and except in the temperature region between 346 and 358 K. Within that 12 K only 18 of the 1105 data points represented in the figure have deviations greater than $\pm 5\%$. The larger deviations in this region are due primarily to the lack of emphasis on fitting the critical region.

The second virial coefficients of Gillis [16] were the only data of that type used in the fit of the MBWR equation. Deviations of the second virial coefficients of Gillis [16] from second virial coefficients calculated with the MBWR equation are all slightly positive, with the bias and A.A.D. both equal to 0.51%. The maximum deviation of the experimental second virial coefficients used in the fit from the MBWR correlation was $2.72\ \text{cm}^3 \cdot \text{mol}^{-1}$.

5.3. Heat Capacity and Speed of Sound

Figure 10 shows the deviations of the Magee isochoric and saturated heat capacities and the Russell et al. [9] near-saturation isobaric heat capacity data from the MBWR equation of state for R143a. The maximum

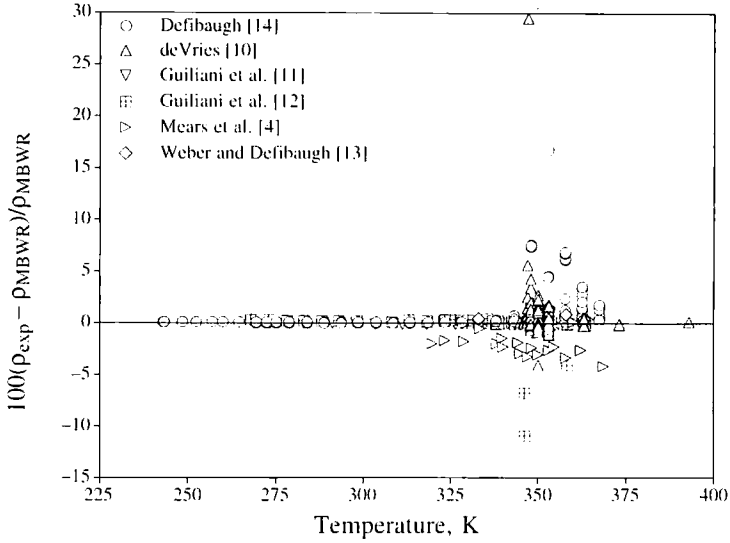

Fig. 8. Deviations of experimental *PVT* data not used in the formulation of the MBWR equation from densities calculated with the MBWR equation as a function of temperature.

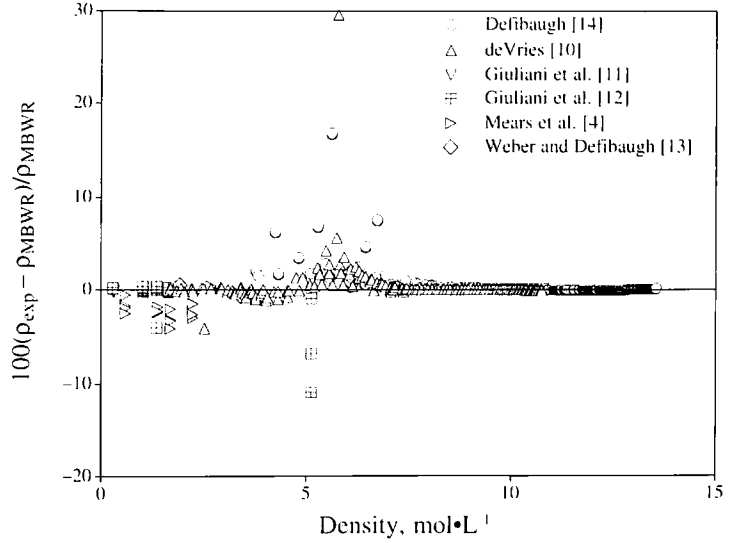

Fig. 9. Deviations of experimental *PVT* data not used in the formulation of the MBWR equation from densities calculated with the MBWR equation as a function of experimental density.

deviation of the isochoric heat capacity C_v is 2.02%. The saturated heat capacity C_σ of Magee [8] is fitted to within $\pm 2.0\%$ except above 333 K. Above 333 K the greatly increased deviations of these data are due in part to their proximity to the critical region and their relationship to the saturation properties (which have their largest deviations as they approach critical). The data of Russell et al. [9] were not given any weight in the formulation of the MBWR equation but are still fitted with a maximum deviation of only 0.35%.

Figure 11 shows the deviations of the experimental speed-of-sound data of Gillis [16] from values calculated with the MBWR equation. These are vapor-phase data taken along isotherms and are fitted to within $\pm 0.15\%$. Table III lists statistics (A.A.D. and bias) for each of the available heat capacity and speed-of-sound data sets.

5.4. Pressure–Temperature Behavior of Heat Capacity and Speed of Sound

To establish that our MBWR correlation represents an accurate thermodynamic surface over the full temperature and pressure ranges of interest, we examine plots of the speed of sound, isochoric heat capacity, and isobaric heat capacity. Figures 12–14 show such plots for our MBWR correlation of R143a from the triple point of R143a (161.82 K) to 500 K and to pressures of 60 MPa. These plots show qualitatively correct behavior for each of the properties with one exception: the speed of sound does not approach 0 at the critical point. This is a common flaw which is associated with analytical equations of state such as the MBWR.

A pressure–enthalpy diagram (shown as Fig. 15) prepared from properties calculated with the MBWR equation for R143a is one final check to make sure our equation is exhibiting reasonable behavior over the temperature and pressure range of interest. (Following common practice, the diagram is on a mass basis, with temperature in degrees Celsius.) Figure 15 shows no signs of abnormal behavior.

6. SUMMARY AND CONCLUSIONS

A 32-term modified Benedict–Webb–Rubin (MBWR) equation of state has been used to correlate experimental, thermodynamic property data for R143a. Experimental data used in this correlation covered temperatures from 162 to 346 K and pressures to 35 MPa. The MBWR correlation of R143a presented here shows good agreement with experimental data except in the immediate vicinity of the critical point. Based on an examination of plots of speed of sound, isochoric heat capacity, and isobaric heat capacity and a pressure–enthalpy diagram, we conclude that our MBWR equation

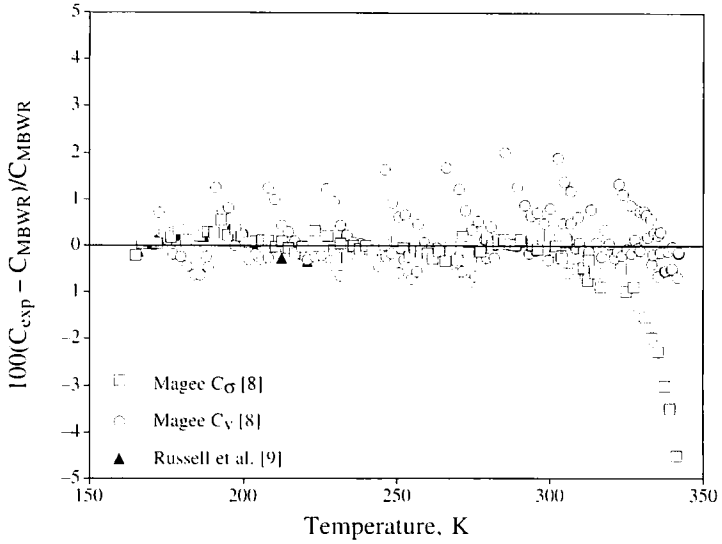

Fig. 10. Deviations of experimental isochoric, isobaric, and saturated liquid heat capacities used in the formulation of the MBWR equation from values calculated with the MBWR equation.

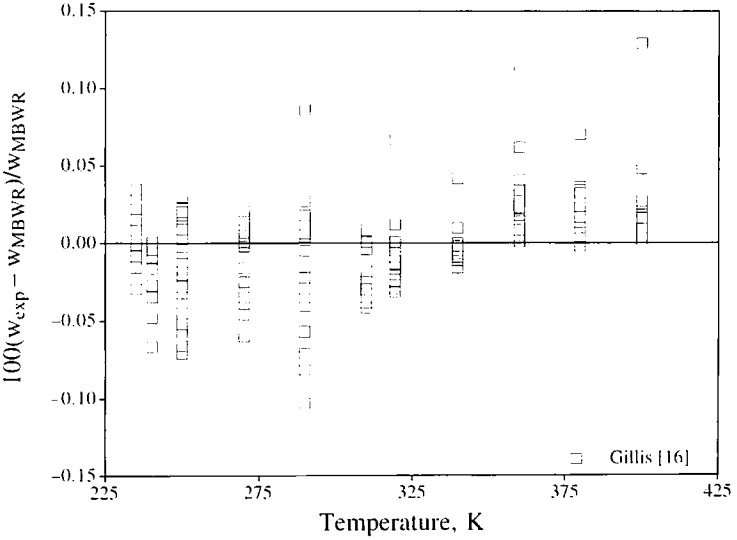

Fig. 11. Deviations of experimental speed-of-sound data from values calculated with the MBWR equation.

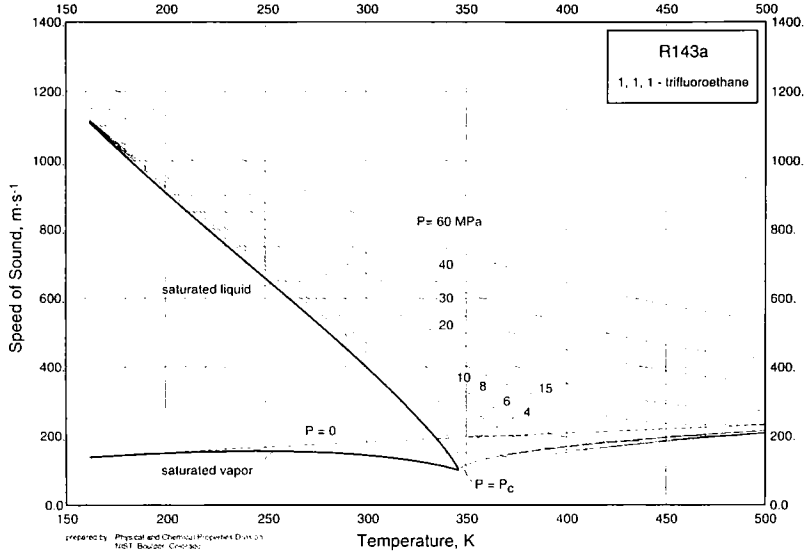

Fig. 12. Speeds of sound calculated with the MBWR equation of state on isobars to 60 MPa.

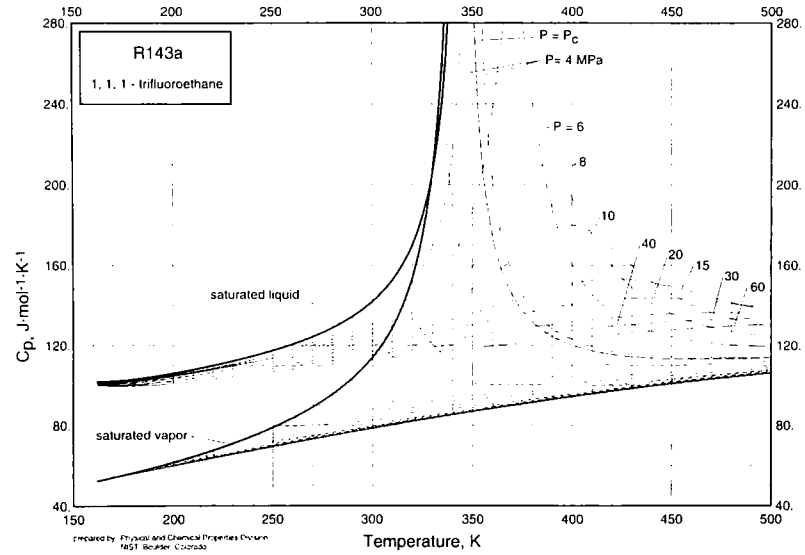

Fig. 13. Isobaric heat capacities calculated with the MBWR equation of state on isobars to 60 MPa.

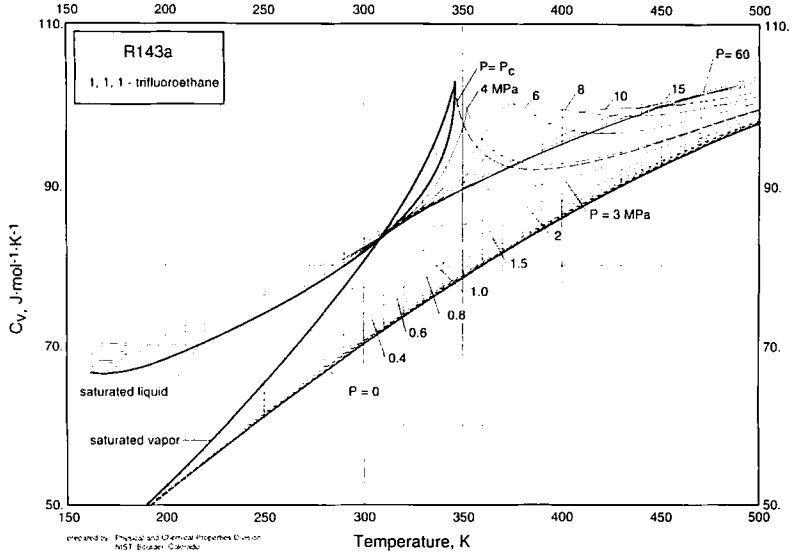

Fig. 14. Isochoric heat capacities calculated with the MBWR equation of state on isobars to 60 MPa.

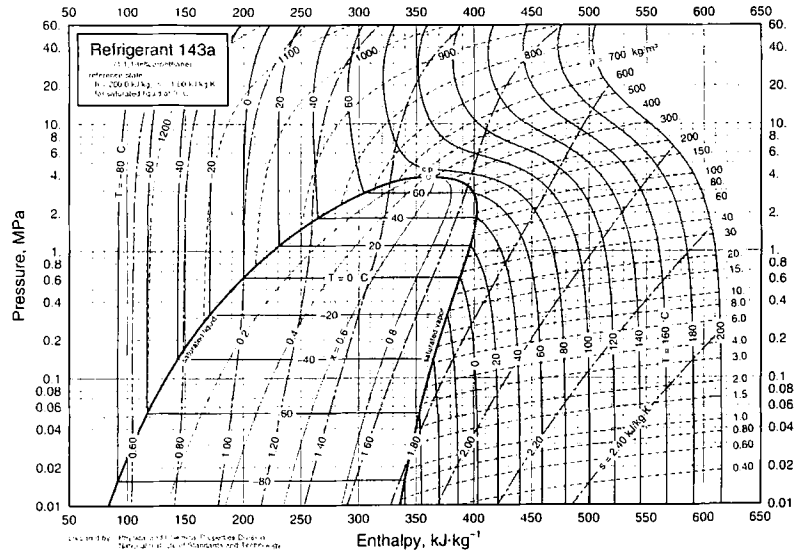

Fig. 15. Pressure-enthalpy diagram for R143a calculated with the MBWR equation.

of state for R143a exhibits thermodynamically reasonable behavior upon extrapolation to 500 K and 60 MPa.

ACKNOWLEDGMENTS

We thank our colleagues at NIST whose data we used before publication: D. R. Defibaugh, K. A. Gillis, C. D. Holcomb, J. W. Magee, J. W. Schmidt, and L. A. Weber. We thank B. de Vries of the University of Hannover, Hannover, Germany, for providing his data before publication. This research project was supported by a grant from the U.S. Department of Energy, Office of Building Technology through the Air Conditioning and Refrigeration Institute (Grant number DE-FG02-91CE23810: Materials Compatibilities and Lubricants Research on CFC-Refrigerant Substitutes).

REFERENCES

1. D. Arnaud, S. Macaudiere, L. Niveau, and S. Wosinski, in *Proceedings of the XVIII International Congress of Refrigeration, Montreal, Canada* (1991), paper 79.
2. M. Fukushima, *Trans. Jpn. Assoc. Refrig.* **10**:87 (1993).
3. Y. Higashi and T. Ikeda, presented at the 4th Asian Thermophysical Properties Conference, Tokyo, Japan, Sept. 5–8, (1995).
4. W. H. Mears, R. F. Stahl, S. R. Orfeo, R. C. Shair, L. F. Kells, W. Thompson, and H. McCann, *Indust. Eng. Chem.* **47**:1449 (1955).
5. M. Nagel and K. Bier, *Int. J. Refrig.* **19**:4 (1996).
6. J. W. Schmidt, personal communication (NIST, Gaithersburg, MD, 1995).
7. H. Wang, Y. Ma, C. Lu, and Y. Tian, *Beijing Gongchang Rewuli Xuebao* (*Chinese J. Eng. Thermophys.*) **14**:124 (1993).
8. J. W. Magee, personal communication (NIST, Boulder, CO, 1996).
9. H. Russell, D. R. V. Golding, and D. M. Yost, *J. Am. Chem. Soc.* **66**:16 (1944).
10. B. de Vries, Thermodynamische Eigenschaften der alternativen Kältemittel R32, R125 und R143a—Messungen und Zustandsgleichungen, Thesis Disertation, University of Hannover, (1996).
11. G. Giuliani, S. Kumar, F. Polonara, and P. Zazzini, *International Conference CFC's, The Day After* (Padua, Italy, 1994), p. 525.
12. G. Giuliani, S. Kumar, P. Zazzini, and F. Polonara, *J. Chem. Eng. Data* **40**:903 (1995).
13. L. A. Weber and D. R. Defibaugh, *J. Chem. Eng. Data* **41**:1477 (1996).
14. D. R. Defibaugh and M. R. Moldover, *J. Chem. Eng. Data* **42**:160 (1997).
15. C. Yokoyama and S. Takahashi, *Fluid Phase Equil.* **67**:227 (1991).
16. K. A. Gillis, *Int. J Thermophys.* **18**:73 (1996).
17. C. D. Holcomb, personal communication (NIST, Boulder, CO, 1996).
18. S. S. Chen, A. S. Rodgers, J. Chao, R. C. Wilhoit, and B. J. Zwolinski, *J. Phys. Chem. Ref. Data* **4**:441 (1975).
19. D. C. Smith, G. M. Brown, J. R. Nielsen, R. M. Smith, and C. Y. Liang, *J. Chem. Phys.* **20**:473 (1952).
20. W. N. Vanderkooi and T. De Vries, *J. Phys. Chem.* **60**:636 (1956).
21. C. M. Bignell and P. J. Dunlop, *J. Chem. Phys.* **98**:4889 (1993).

22. M. R. Moldover, J. P. M. Trusler, T. J. Edwards, J. B. Mehl, and R. S. Davis, *J. Res. Natl. Bur. Stand. (U.S.)* **93**:85 (1988).
23. D. G. Friend, J. F. Ely, and H. Ingham, *J. Phys. Chem. Ref. Data* **18**:583 (1989).
24. L. A. Weber, *International Refrigeration Conference*, West Lafayette, IN, July 14–17 (1992), p. 463.
25. R. T. Jacobsen and R. B. Stewart, *J. Phys. Chem. Ref. Data* **2**:757 (1973).
26. B. A. Younglove and J. F. Ely, *J. Phys. Chem. Ref. Data* **16**:577 (1987).
27. B. A. Younglove, *J. Phys. Chem. Ref. Data* **11** (1982).
28. B. A. Younglove and M. O. McLinden, *J. Phys. Chem. Ref. Data* **23**:731 (1994).